HHS Public Access

Author manuscript

J Am Chem Soc. Author manuscript; available in PMC 2020 January 09.

Published in final edited form as:

J Am Chem Soc. 2019 January 09; 141(1): 204–215. doi:10.1021/jacs.8b08243.

Contribution of Cotranslational Folding Defects to Membrane Protein Homeostasis

Francis J. Roushar[†], **Timothy C. Gruenhagen**[†], **Wesley D. Penn**[†], **Bian Li**[‡], **Jens Meiler**[‡], **Beata Jastrzebska**[§], and **Jonathan P. Schlebach**[*,†]

[†]Department of Chemistry, Indiana University, Bloomington, Indiana 47405, United States

[‡]Department of Chemistry, Vanderbilt University, Nashville, Tennessee 37235, United States

[§]Department of Pharmacology, Case Western Reserve University, Cleveland, Ohio 44106, United States

Abstract

Membrane proteins are prone to misfolding and degradation within the cell, yet the nature of the conformational defects involved in this process remain poorly understood. The earliest stages of membrane protein folding are mediated by the Sec61 translocon, a molecular machine that facilitates the lateral partitioning of the polypeptide into the membrane. Proper membrane integration is an essential prerequisite for folding of the nascent chain. However, the marginal energetic drivers of this reaction suggest the translocon may operate with modest fidelity. In this work, we employed biophysical modeling in conjunction with quantitative biochemical measurements in order to evaluate the extent to which cotranslational folding defects influence membrane protein homeostasis. Protein engineering was employed to selectively perturb the topological energetics of human rhodopsin, and the expression and cellular trafficking of engineered variants were quantitatively compared. Our results reveal clear relationships between topological energetics and the efficiency of rhodopsin biogenesis, which appears to be limited by the propensity of a polar transmembrane domain to achieve its correct topological orientation. Though the polarity of this segment is functionally constrained, we find that its topology can be stabilized in a manner that enhances biogenesis without compromising the functional properties of rhodopsin. Furthermore, sequence alignments reveal this topological instability has been conserved throughout the course of evolution. These results suggest that topological defects significantly contribute to the inefficiency of membrane protein folding in the cell. Additionally, our findings suggest that the marginal stability of rhodopsin may represent an evolved trait.

Graphical Abstract

[*]**Corresponding Author** jschleba@indiana.edu.

Notes

The authors declare no competing financial interest.

ASSOCIATED CONTENT

Supporting Information

The Supporting Information is available free of charge on the ACS Publications website at DOI: 10.1021/jacs.8b08243.

Figures S1−S7, Table S1, Supplemental Theory (PDF)

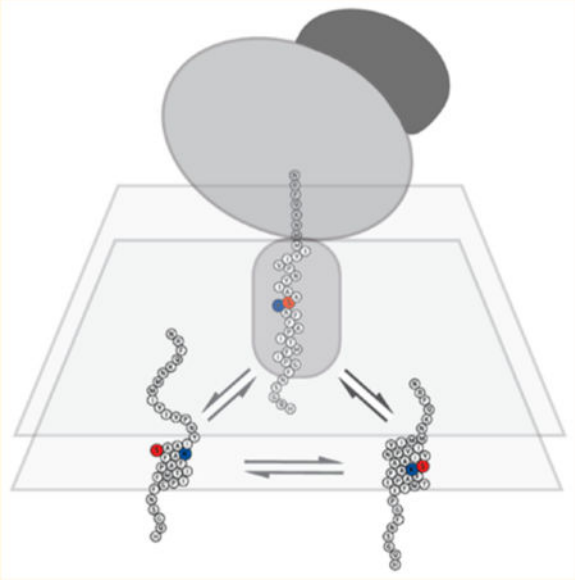

INTRODUCTION

Most eukaryotic membrane proteins must traverse the secretory pathway in order to reach the plasma membrane and carry out their biochemical function. The efficiency of this process depends on the conformational stability of the protein and the corresponding manner in which it interacts with the molecular chaperones of the cellular proteostasis network.[1] Nascent membrane proteins tend to interact avidly with molecular chaperones,[2–4] and as a result, their passage through the secretory pathway is typically inefficient.[5,6] The nature of these interactions suggests membrane proteins are predisposed to conformational defects, yet the structural lesions responsible for these interactions remain poorly understood. Investigations of pathogenic mutations associated with diseases of membrane proteostasis have provided opportunities to explore the spectrum of conformational defects involved in membrane protein misfolding.[5,7] In many cases, the proteostatic effects of these mutations arise from their effects on post-translational folding and/or oligomerization reactions.[6,8–10] However, a survey of pathogenic mutations within integral membrane proteins also identified a subset that are instead likely to compromise cotranslational folding.[11] These cotranslational folding reactions are known to play a critical role in membrane protein folding in the cell.[12–14] Nevertheless, to our knowledge, the fidelity of cotranslational folding has not been rigorously assessed in relation to the cellular proteostasis of integral membrane proteins.

Integral membrane protein folding begins during the cotranslational insertion of the nascent polypeptide into the ER membrane in a manner that is mediated by the Sec61 translocon. This process (topogenesis) establishes the topology of the nascent protein with respect to the membrane, which in turn dictates the portions of the molecule that are exposed to chaperones in the cytosol, the ER lumen, and within the ER membrane itself.[15] Topogenesis is primarily driven by the energetics associated with the partitioning of the nascent chain from the translocon into the membrane;[16–19] a process that occurs with considerable

efficiency for hydro-phobic transmembrane (TM) domains.[17] Nevertheless, it has been estimated that ~25% of TM domains within polytopic membrane proteins are too polar to spontaneously partition into the membrane in the absence of other stabilizing interactions.[16] TM segments that are ill-adapted to the membrane generate topological frustration within the nascent chain,[20] which may compromise the fidelity of topogenesis. In some instances, these polar segments are initially shunted into the aqueous phase then subsequently pulled into the membrane during posttranslational folding.[21–24] In other cases, the membrane integration of polar segments occurs with marginal efficiency, which leads to the formation of a heterogeneous topological ensemble.[25,26] Regardless of whether the native topology is established during or after translation, aberrant topomers appear to be rapidly degraded in the cell.[13,14] However, the extent to which the formation, recognition, and degradation of aberrant topomers contributes to the misfolding and cellular mistrafficking of polytopic membrane proteins is unclear.

In this work, we quantitatively assess the linkage between the fidelity of topogenesis and the outcomes of membrane protein biogenesis. To interrogate this connection, we investigated the topological energetics and cellular trafficking of human rhodopsin, a G-protein coupled receptor (GPCR) that plays an essential role in vision (Figure 1A). The apoform of the protein (opsin) must bind to its 11-cis-retinal cofactor in order to mediate coupling between the photoisomerization of retinal and the initiation of G-protein signaling. Retinal is conjugated to the protein through a Schiff base with a lysine side chain (K296) that is positioned near the center of rhodopsin's seventh TM domain (TM7). Though this residue is essential for function, K296 enhances the polarity of TM7 in a manner that potentially poses a challenge to the fidelity of topogenesis. This physicochemical conflict makes rhodopsin an ideal model system for the investigation of the connection between the topological energy landscape and membrane proteostasis. In the following, we show that activity of the proteostasis network is exquisitely sensitive to the topological energetics of TM7. These findings provide insights into the mechanism by which certain loss-of-function mutations in the rhodopsin gene induce misfolding, which is involved in the molecular basis of autosomal dominant retinitis pigmentosa (adRP).[27] Furthermore, an evolutionary analysis suggests the topological instability of rhodopsin has been conserved throughout the course of evolution. Together our findings implicate topological defects in the cellular misfolding of integral membrane proteins, and suggest additional roles for topo-logical energetics in membrane protein evolution and the molecular basis of disease.

RESULTS

Topological Frustration in Human Rhodopsin.

Rhodopsin adopts a canonical GPCR fold (Figure 1A) featuring seven TM helices that exhibit considerable variations in hydrophobicity. To survey the extent to which these variations impact the topological energetics of rhodopsin, we scanned its sequence using a knowledge-based algorithm that predicts the energetics associated with the transfer of TM helices from the translocon to the ER membrane (ΔG predictor).[16] Sequence scans faithfully identify the first six TM domains of rhodopsin, but suggest that TM7 is not sufficiently hydrophobic to spontaneously partition from the translocon into the membrane (ΔG = +3.5

kcal/mol, Figure 1B). Though the selection of TM7 by the translocon is predicted to be inefficient, it should be noted that the transfer of this segment from the aqueous phase to the membrane core is predicted to be quite favorable according to the Wimley−White water−octanol scale (ΔG = −8.0 kcal/mol).[28] Together these predictions suggest that, though TM7 may be thermodynamically stable within a bilayer, its translocon-mediated membrane integration is likely inefficient. To test the latter prediction, we evaluated the translocon mediated membrane integration of TM7 using a leader peptidase (Lep)-based translocation assay.[29] Briefly, the sequence of TM7 (residues 286−309) was introduced into a chimeric Lep protein, which was then produced by in vitro translation in the presence of canine rough microsomes. Using this approach, an apparent equilibrium constant for membrane integration can be inferred from the relative abundance of singly (TM7 in the membrane) and doubly (TM7 in the lumen) glycosylated translation products.[29] The glycosylation state of this chimeric Lep protein confirms the membrane integration of TM7 occurs with marginal efficiency (29 ± 7%, ΔG_{app} = 0.6 ± 0.2 kcal/mol, Figure 1C). The membrane integration of TM7 appears more efficient than would be expected on the basis of predictions. However, it seems likely that this constitutes an overestimation of the true efficiency given that this measurement is near the limit of the dynamic range of this assay.[23,29] Despite this limitation, this result clearly confirms that TM7 is not efficiently recognized as a TM helix by the translocon during topogenesis.

The inefficient recognition of TM7 by the translocon is likely to result in the formation of non-native topomers. To identify the non-native topological states that are most likely to form, we analyzed the sequence of rhodopsin using a graphical algorithm that predicts the most energetically favorable topologies based on sequence (TopGraph).[30] Consistent with the ΔG predictor, TopGraph suggests the first six TM domains are embedded within the membrane in the context of the two most favorable topologies (Figure 1D). However, TM7 is shunted into the ER lumen in one of the two topologies, which we have termed the misfolded state (M, Figure 1D). TopGraph also suggests the protein is likely to sample a topology in which TM7 traverses the membrane in a manner that places K296 among the anionic lipid head groups of the inner membrane leaflet. Because K296 is out of position and the TM domain is shorter than TM7 appears in a homology model of human rhodopsin (Figure 1A), we have termed this the near-native state (N*, Figure 1D). To facilitate proper folding, we reason that TM7 must lengthen and shift with respect to the membrane to form an additional topological state (N) in which K296 is natively positioned within the protein core (Figure 1D). These predictions suggest TM7 can adopt at least two distinct orientations within the membrane that differ with respect to length and position. To evaluate whether frustration in this segment gives rise to alternative energetic minima, we scanned the TM7 region to identify nascent TM segments of variable length using the ΔG predictor. Two distinct yet isoenergetic minima can be observed in the 19-residue and 24-residue window scans, which also suggest the translocon is equally likely to recognize TM7 in the N (24-residue helix centered at residue 297) or N* orientation (19-residue helix centered at residue 291) (predicted $\Delta\Delta G_{N-N^*}$ = 0.0 kcal/mol, Figure 2A). To test this prediction, the 19-residue segment (residues 283−301) corresponding to this alternative energetic minimum was introduced into a chimeric Lep protein, which was then characterized by in vitro translation. Consistent with predictions, the apparent efficiency associated with the membrane

integration of this segment (22 ± 4%) is indistinguishable from that of native TM7 (Figure 1C). Together, these results suggest topological frustration within TM7 may drive the formation of multiple topologies during rhodopsin biogenesis.

To probe the extent to which topological frustration impacts the nascent ensemble, we utilized in vitro translation in conjunction with limited proteolysis in order to probe the topological properties of full-length rhodopsin in a manner described previously.[31] Briefly, a tobacco etch virus (TEV) protease-cleavable reporter domain was genetically fused to the C-terminus of rhodopsin, and the fusion protein was translated within canine rough microsomes. The nascent protein was then digested with TEV protease to determine whether TM7 exhibits a pattern of proteolytic protection that is consistent with the formation of multiple topologies (Figure S1). The glycosylated opsin band, which is properly processed and targeted to the membrane, exhibits partial protection from proteolysis (Figure S1). Furthermore, this protected fraction is digested in the presence of a membrane-permeabilizing detergent (Figure S1), which confirms the proteolytic protection arises from the aberrant localization of the C-terminus within the microsomal lumen. The incomplete digestion of the nascent opsin band suggests at least two topomers are produced during translation; one in which TM7 is within the microsomal lumen (i.e., the M state) and one in which TM7 traverses the membrane (i.e., the N* and/or N state). It should be noted that the fraction of cleavable protein (~70%) exceeds the membrane integration efficiency of TM7 in the context of the Lep protein (Figure 1C). This observation suggests the transfer free energy of TM7 may be partially offset in the context of the full-length protein through formation of interhelical contacts at the translocon.[32,33] Nevertheless, these data confirm TM7 adopts multiple topologies within the nascent conformational ensemble of opsin.

Engineering the Topological Energy Landscape of Rhodopsin.

Our results suggest the propensity of opsin to sample non-native topologies arises from the sequence of TM7 and its corresponding topological frustration. To explore the relevance of this frustration to rhodopsin misfolding, we first utilized structural modeling and energetics algorithms to design a series of rhodopsin TM7 variants with selectively modified topological energetics. To identify a position within TM7 that is amenable to protein engineering, we constructed a structural homology model of human rhodopsin based on the structure of bovine rhodopsin (93.4% sequence identity, Figure 1A). In both the bovine structure and the human model, we find that residue 297 (a serine in human rhodopsin) forms no apparent tertiary contacts and projects into the membrane core (Figure 1A). Thus, substitutions at this position should alter the transfer free energy of TM7 without appreciably disrupting the native structure. To confirm that mutations are likely to be tolerated at this position, we constructed and analyzed a series of structural models for variants containing mutations at residue 297. A comparison of the lowest energy models of mutant proteins all exhibit root-mean-square deviation (RMSD) values of less than 0.4 Å relative to the model of WT, which confirms the native, functional fold can accommodate a range of amino acids at this position (Figure S2). Moreover, the calculated effects of these mutations on Rosetta energies are dominated by membrane solvation parameters (Table S1A), which again suggests these mutations primarily impact the energetics of solvation within the membrane. With the exception of S297W, which is predicted to be stabilizing,

Rosetta energies suggest these substitutions should have minimal effect of the conformational stability of rhodopsin (Table S1A). Though these results suggest mutations to residue 297 should not significantly impact the structure or stability of the native topomer, it should be noted that the mutation of this residue to an arginine causes adRP. Thus, the cellular proteostasis of rhodopsin is still likely to be sensitive to energetic perturbations at this position.

Energetic predictors provide a means of rationalizing the effects of mutations on the nascent topological ensemble of TM7. In the context of the predicted topomers, serine 297 resides within the aqueous phase in the M state, the membrane interface in the N* state, and within the membrane core in the N state (Figure 1D). Thus, changes in the hydrophobicity of this side chain alter the energetics of topogenesis in a manner that should skew the ratio of nascent topomers. Indeed, sequence scans of a series of residue 297 variants suggest mutations at this position influence both the probability associated with the recognition of TM7 by the translocon as well as the most favorable position of this helix within the membrane (Figure 2A,B). To estimate the effects of mutations on the nascent topological ensemble, we used a three-state equilibrium model to interpret energetic predictions by making the simplifying assumption that the failure of TM7 to enter the membrane during translation results in the formation of the M state (Figure 2C). Briefly, we first utilized our experimental measurements of the membrane integration efficiency of TM7 (Figure 1C) to calculate apparent free energy differences between the M, N*, and N topomers for the WT protein. We next utilized the ΔG predictor to calculate the effects of mutations on the free energy difference between each state based on depth-dependent transfer free energies for each side chain (Table 1). We then used these estimated ΔΔG values in conjunction with a three-state equilibrium model to recalculate the predicted fraction of each topomer (Supplemental Theory, Table 1). Despite limitations in the dynamic range of Lep-based measurements (described above), we find the predictions generated by this model to be correlated with the apparent mutagenic effects on the membrane integration efficiency of TM7 (Pearson's R = 0.73, Figure S3). Inclusion of the N* state in the equilibrium model improves predictions for the effects of charged substitutions at residue 297 relative to those generated using a two state equilibrium model (Figure S3). The predicted fraction of native topomer (f_N) is only 0.14 within the WT ensemble, with mutant f_N values ranging from 0.04 (S297K) to 0.32 (S297L) (Table 1). Interestingly, the introduction of charged residues at residue 297 is predicted to stabilize the N* state. For instance, the S297R mutation is predicted to decrease f_N from 0.14 to 0.05 while increasing the fraction of the near-native topomer (f_{N*}) from 0.15 to 0.19. This stabilization arises from differences in the depth-dependent transfer free energies of charged amino acid side chains.[16,34–36] Together, these computational results provide a useful lens for the interpretation of mutagenic effects as well as plausible estimates for the effects of mutations on the nascent topological ensemble.

Influence of Topological Energetics on Rhodopsin Proteostasis.

Mutations that selectively perturb topological energetics provide a unique opportunity to investigate the extent to which topological defects contribute to membrane protein misfolding in the cell. The misfolding of integral membrane proteins typically results in their retention within the early secretory pathway and/or their premature degradation within

the cell. Therefore, to determine whether the activity of the proteostasis network is sensitive to the topological energetics of TM7, we quantitatively compared the expression levels and cellular trafficking of engineered opsin variants by flow cytometry as described previously.[6] Briefly, each variant was transiently expressed in HEK293 cells prior to the selective immunostaining of plasma membrane opsin (mature) and intracellular opsin (immature) with distinct fluorophores. Flow cytometry was then employed to quantitatively compare the immunostaining patterns of each variant. Though mutagenic trends were consistent, the proportion of surface protein relative to total protein (export efficiency) was found to vary between batches of cells and with increasing passage number. A comparison of plasma membrane and intracellular immunostaining levels for a single batch of cells at low passage number reveals that only 24 ± 2% of cellular WT opsin is present at the plasma membrane. As is true for many other eukaryotic membrane proteins,[5,6] this marginal trafficking suggests opsin is prone to misfolding and is inefficiently exported from the secretory pathway. Both surface and total cellular opsin immunostaining levels are highly sensitive to mutations at residue 297 (Figure 3A,B), which suggests the topological energetics of rhodopsin are tightly linked to the folding efficiency of cellular rhodopsin. By comparison, similar mutations within more hydrophobic TM domains have minimal impact on steady-state opsin levels (Figure S4), which further implicates the topological frustration of TM7 in opsin misfolding. The accumulation of opsin variants in the cell and at the plasma membrane is generally proportional to predicted f_N values (Figure S5). Moreover, with the exception of S297D and S297R, predicted f_N values for these variants are tightly correlated with the efficiency of their export from the secretory pathway to the plasma membrane (Figure 3C). The aberrant trafficking of S297D and S297R opsin may reflect inaccuracies in the predicted energetic effects of these mutations on the structural and/or topological ensemble, or differences in the manner in which these variants are recognized by molecular chaperones. Nevertheless, these results demonstrate that the activity of the proteostasis network is highly sensitive to the topological energetics of TM7. Though it is possible that these mutations may influence other conformational properties of rhodopsin, the proteostatic effects of these substitutions appear to be well-described by their predicted impacts on the nascent topological ensemble.

It is possible that other physiochemical factors may suppress the formation of aberrant topomers in vivo. In particular, cofactor binding can have a profound effect on membrane protein folding and assembly in the cell.[6] Retinal binding is known to stabilize rhodopsin in a manner that increases its cellular expression and trafficking.[37] However, it is unclear whether the nascent topological ensemble is sensitive to the effects of retinal binding. Considering the N state is the only putative topomer capable of forming the native retinal binding pocket, we reason this topology should be selectively stabilized in the presence of retinal (Figure 1D). On the basis of the binding affinity of retinal (K_d ~ 25 pM),[38] we estimate that low micromolar concentrations of this cofactor should thermodynamically stabilize the native topomer by >6 kcal/ mol relative to the ensemble of non-native topomers that lack a binding pocket an effect far greater than the predicted effects of mutations (Table 1). Thus, provided these topomers are capable of exchanging on physiological time scales, we would expect binding to compensate for the modest energetic effects of these mutations. To assess the proteostatic effects of cofactor binding, we compared the expression and

trafficking of rhodopsin variants in the presence and absence of 5 μM of the isochromophore 9-*cis*-retinal. The surface and total protein immunostaining levels of WT rhodopsin increase by 14 ± 13% and 14 ± 6% in the presence of retinal, respectively, which confirms the stabilization of isorhodopsin by retinal influences proteostasis. A comparison of the immunostaining profiles of cells grown in the presence and absence of retinal reveals that, with the exception of S297R, the expression and trafficking of each variant is increased by a similar magnitude (Figure 4). By comparison, the S297R variant, which significantly increases the topological frustration of TM7 (Supplemental Theory), exhibits no statistically significant response to retinal. The persistence of the proteostatic effects of topologically stabilizing and destabilizing mutations in the presence of retinal demonstrates that cofactor binding does not alter the topological energetics of isorhodopsin. The effects of retinal are instead likely to arise from its effects on the posttranslational folding efficiency of the native topomer. This finding is consistent with recent reports that the topological ensemble is also insensitive to the energetics of dimerization.[39] Taken together, these observations suggest the proteostatic effects of retinal binding are unlikely to involve the fidelity of cotranslational folding.

Functional Properties of Engineered Rhodopsin Variants.

Several of these engineered opsin variants enhance the yield of mature opsin at the plasma membrane (S297L, S297A, and S297W, Table 1). Assuming selection pressures serve to maximize the yield of functional rhodopsin, we suspected that these mutations should have adverse effects on the functional properties of rhodopsin. To evaluate the effects of these mutations on rhodopsin function, 11-cis-retinal was added to HEK293 cells transiently expressing each variant in order to regenerate rhodopsin. Regenerated rhodopsin pigments were then purified and functionally characterized. We compared the UV−visible spectra of purified rhodopsin variants before and after exposure to light, the kinetics of retinal release following illumination (meta II decay), and the kinetics of G_t activation for each mutant, as was described previously.[40–42] Relative to WT, S297W rhodopsin exhibits an attenuated chromophore binding, severe retardation of meta II decay, and an inability to activate G_t (Table 2, Figure S6). Similarly, the S297A variant is capable of activating G_t, but still has mild adverse effects on the spectral properties and meta II decay kinetics (Table 2, Figure S6). These results confirm that S297W and S297A have negative impacts on the fitness of rhodopsin. However, the S297L variant, which improves the yield of mature protein at the plasma membrane by 34 ± 7%, has no discernible effects on the spectral properties of rhodopsin (Figure 5A), its meta II decay kinetics (Figure 5B), or its G_t-mediated signaling (Figure 5C, Table 2). Thus, S297L enhances the efficiency of rhodopsin biogenesis with no apparent impact on function. This finding demonstrates that the polarity of TM7 does not entirely arise as a consequence of the sequence constraints of rhodopsin function.

Evolutionary Constraints on the Topological Energetics of Rhodopsin.

The polarity of TM7 appears to limit the expression and maturation of opsin within the secretory pathway (Figure 3C). Thus, the appearance of a functionally silent polar residue at position 297 suggests that the polarity of TM7, and by extension the inefficient biogenesis of rhodopsin, may confer an evolutionary benefit. To evaluate the extent to which the topological energetics are conserved, we compared the sequences of TM7 among 104

rhodopsin proteins. As expected, the functionally essential K296, which forms a Schiff base with its 11-cis-retinal cofactor, is absolutely conserved (Figure 6A). Interestingly, we find that most TM7 sequences contain a string of three serine residues near the center of the TM domain, which reveals that many forms of TM7 are considerably more polar than that of human rhodopsin (Figure 6A). To determine the extent to which the topological energetics of TM7 have been constrained, we scanned these sequences using the G predictor.[16] Sequence scans reveal that TM7 sequences exhibit wide variations in transfer free energy (ΔG_{N-M}) but are, without exception, exceedingly polar (Figure 6B). These high transfer free energies cannot be solely attributed to functionally essential polar residues (Figure S7). Though we cannot rule out that the true energetics deviate from predictions, these results suggest selection pressures have not constrained the hydrophobicity of TM7 in a manner that maximizes the expression level of opsin. It should be noted, however, that a comparison of sequence scans reveals little variation in the free energy difference between the near-native and native topomers (ΔG_{N-N*}, Figure 6B), which suggests the sequence of TM7 and its N-terminal loop have been constrained to promote the proper positioning of the helix within the membrane. Indeed, the margin for error in this transition appears to be quite thin considering the S297R variant, which exhibits the largest reduction in surface opsin and is known to cause adRP, would represent an outlier relative to natural TM7 sequences (predicted G_{N-N*} = 0.81 kcal/mol, Figure 6B). Nevertheless, the preservation of the suboptimal topological energetics of TM7 suggests its sequence appears to have been constrained in a manner that preserves its marginal topological energetics and the inefficient folding of cellular rhodopsin.

DISCUSSION

The earliest steps of integral membrane protein folding and misfolding occur during translation and are mediated by the translocon. The translocon-mediated membrane integration of the nascent chain facilitates the formation of the native topology, which is a critical prerequisite for proper folding of membrane proteins in the cell.[5] In this work, we evaluated the fidelity of this process in relation to the cellular misfolding of polytopic membrane proteins. Using rhodopsin as a model system, we assessed the extent to which the propensity of the nascent chain to form non-native topomers ultimately influences its expression and maturation. Energetics-based algorithms[16,30] identify TM7 as a likely source of topological frustration. We then used these algorithms to engineer a series of TM7 variants with selectively modified topological energetics, and characterized their expression and maturation within the cell. Our results reveal the topological preferences of TM7 have a sizable effect on the efficiency with which rhodopsin is exported from the secretory pathway to the plasma membrane (Figure 3B,C). These results parallel recent reports linking the membrane integration efficiency of TM domains to the heterologous expression levels of membrane proteins in bacteria.[43,44] Given that polar TM domains are relatively common among polytopic membrane proteins,[16,45] these results suggest the fidelity of topogenesis may often impose a bottleneck on the efficiency of membrane protein folding in the cell. Furthermore, many mutations associated with diseases of membrane protein misfolding are predicted to enhance the topological frustration of the nascent chain.[11] Additional investigations are needed to elucidate the mechanism by which aberrant topomers are

recognized by the proteostasis network, and the role of this process in diseases of membrane proteostasis.

The segments of the nascent chain that are most likely to undergo translocon-mediated membrane integration are often distinct from native TM helices,[21] and certain TM domains must rely on post-translational folding reactions to achieve the correct topology.[23,24,26] In the context of rhodopsin, energetic predictors primarily suggest that the membrane integration of TM7 is likely inefficient and that the polar residues within this segment are likely to stabilize a non-native orientation of TM7 with respect to the membrane (the N* state, Figure 1D). The output of the G predictor[16] and TopGraph[30] differ with respect to energetics and the predicted length of TM7 in this near-native topomer. Nevertheless, the fact that each identify this putative topological state is remarkable considering these algorithms utilize distinct methodologies and energy scoring systems that are derived from unrelated data.[16,29,30,36] The relative stability of this putative topomer, the formation of which is confirmed by an in vitro translocation assay (Figure 1C), arises as a consequence of the depth-dependent transfer free energies of the polar residues within TM7 and a corresponding reduction in free energy associated with the movement of polar residues toward the hydrated membrane interface.[16,34–36] This topomer may also be stabilized by the snorkeling of K296 into the inner membrane leaflet and the formation of electrostatic interactions with anionic lipid head groups (the Positive-Inside rule).[18,46] The strengthening of such interactions by the S297R variant, which exhibits severe misfolding and is the only mutation within the series known to cause adRP, is projected to selectively stabilize of the N* state (Figure 2B). Thus, in the case of this mutation, the disruption of topological energetics appears likely to directly contribute to the molecular basis of disease. Nevertheless, it should be noted that both S297R and S297D exhibit larger reductions in export efficiency than would be expected based on topological predictions (Figure 3C). This deviation may suggest the transfer free energy of these TM7 variants may deviate from the predictions, or perhaps that these substitutions disrupt the conformational equilibrium of rhodopsin in other ways. It could also be that the introduction of these charged residues alters the nature in which the nascent chain interacts with ER quality control machinery. Additional studies are needed to gain further insights into the mechanisms by which aberrant topomers interact with molecular chaperones.

The opsin apo protein exhibits an extremely high affinity for retinal (K_d ~ 25 pM),[38] and retinal binding shifts its conformational equilibrium in a manner that enhances the cellular expression and trafficking of rhodopsin.[37] Retinal and retinal analogues may therefore have the capacity to serve as pharmacological chaperones that bind and stabilize misfolded rhodopsin variants associated with adRP.[27,47,48] Though this strategy is potentially applicable to a wide array of proteostatic diseases,[49,50] it is unclear which types of conformational defects can be corrected by this class of compounds.[5] Our findings demonstrate that retinal binding is incapable of compensating for mutagenic perturbations of the topological energetics, which suggests the binding of small molecules may have a limited influence on the fidelity of topogenesis. Indeed, the only variant that exhibits no detectable response to retinal is S297R (Figure 4), which is predicted to severely augment the topological frustration of TM7 (Table 1, Supplemental Theory). This outcome is perhaps intuitive considering the retinal binding pocket cannot be completed without the proper

membrane integration of TM7. Furthermore, this could potentially provide an explanation for the observation that pharmacological chaperones are not equally efficacious toward the entire spectrum of variants capable of inducing membrane protein misfolding.[51,52] Regardless of this shortcoming, the recent clinical approval of Lumacaftor and Tezacaftor for the treatment of cystic fibrosis[53–55] provides a source of optimism for the development of novel pharmacological chaperones. Further investigations into the influence of binding reactions on the conformational equilibria and cellular proteostasis of integral membrane proteins are needed to gain insights into the pharmacological mechanisms of these compounds.

Our results also have implications for the role of topological energetics in the evolution of integral membrane proteins. It has been widely assumed that marginal conformational stability may represent an emergent property of natural proteins that have evolved to maximize function.[56] Indeed, mutations that lock a protein into a specific conformation may often suppress the conformational motions that mediate protein function. In this regard, it is perhaps unsurprising that the wild-type sequence of rhodopsin can be rationally engineered to enhance its maturation within the cell. However, our findings suggest that much of this instability arises from topological energetics, a property with no explicit connection to functional dynamics. If enhanced expression and maturation provides a fitness benefit, it seems likely that there should be many ways to reduce the topological frustration in TM7 without compromising the function of rhodopsin. Indeed, our finding that the S297L mutation increases the yield of mature protein in the cell without adverse effects on function suggests the topological frustration within TM7 cannot be entirely attributed to functional constraints (Figure 5, Figure S7). Though our experiments may not capture the entire range of physiological effects of mutations in rhodopsin, the relative conservation of a nonessential polar residue at position 297 suggests the instability of the native topomer may represent a selected trait of the rhodopsin protein. Such a conclusion is not without precedent; there is some evidence to suggest selection pressures have compromised the conformational stability of the mammalian gonadotropin-releasing hormone receptor (GnRHR).[57] On the basis of these previous findings, it has been suggested that the marginal conformational stability of this receptor may provide a regulatory benefit.[58] Indeed, given the intrinsic propensity of integral membrane proteins to misfold, it stands to reason that changes in the concentrations and/or activity of molecular chaperones may serve to tune the efficiency with which they are exported from the ER.[59] Additional investigations are needed to gain insights into the interface between topological energetics and cellular quality control, and how these factors contribute to the evolution of integral membrane proteins.

EXPERIMENTAL SECTION

Computational Predictions of Topological Energetics.

Transfer free energy predictions associated with the membrane integration of nascent proteins were generated using the ΔG predictor algorithm (http://dgpred.cbr.su.se/), a knowledge-based algorithm that predicts the apparent transfer free energy of a segment from the translocon to the membrane based on amino acid sequence.[16,29] These predictions are generated by summing depth-dependent transfer free energies for each amino acid within

each possible TM segment. Sequence scans carried out in this manner, which evaluate predicted transfer free energies as a function of the length and position of each putative TM domain, were used to identify the segments of the protein that are most likely to undergo translocon-mediated membrane integration. Topological energy landscape predictions associated with longer segments within the TM7 region (i.e., Figure 2A,B) were generated with predictions from a series of individual segments rather than from full sequence scans. Topological predictions associated with full-length rhodopsin (Figure 1D) were generated using TOPGRAPH (http://topgraph.weizmann.ac.il).[30] Natural rhodopsin variants were gathered from the UniProt database (https://www.uniprot.org) and aligned using Clustal Omega (https://www.ebi.ac.uk/Tools/msa/clustalo/). Predicted ΔG values associated with the formation of the N-state (24-residue window) and the N* state (19-residue window) of each natural TM7 region were then generated for each natural sequence using the ΔG predictor algorithm.

Structural Modeling of Human Rhodopsin Variants.

Homology models of the wild-type human rhodopsin (UniProtKB P08100) were constructed based on a crystallographic structure of bovine rhodopsin (PDB ID 3C9L, 2.6 Å resolution, 93.4% sequence identity) using the RosettaCM comparative modeling algorithm.[60] The starting (partial) model was generated by threading the sequence of human rhodopsin onto the structure of bovine rhodopsin in a manner guided by their sequence alignment. Conformations of fragments in the starting model where coordinates are missing were then modeled by Monte Carlo sampling from a Rosetta de novo modeling fragment database selected from the Protein Data Bank using local sequence information.[61] Sampling was guided using a Rosetta energy function adapted for membrane proteins. The boundaries of membrane-spanning segments, as required by membrane protein-specific terms in the Rosetta energy function, were extracted from the OPM database.[62] 5000 structural models were generated and clustered. The lowest-energy model from the largest cluster was then selected as the final model for the WT human rhodopsin. To construct models for the eight variants of human rhodopsin studied experimentally (S297A, S297D, S297E, S297K, S297L, S297N, S297R, S297W), the wild-type serine residue was first replaced with a plausible rotamer of the corresponding variant residue. The resulting variant model was then relaxed using the Rosetta energy function. 100 models were then generated for each variant, and the model with the lowest energy was selected as the final model. The effects of each mutation on the thermodynamic stability of rhodopsin were also computationally estimated using the a Rosetta energy function optimized for membrane proteins in conjunction with Rosetta ΔΔG protocol.[63] This protocol optimizes both the initial input model for the wild-type and the generated model for the variant in the same way for 50 iterations. The ΔΔG for each variant is then calculated as $\Delta\Delta G = \Delta G_{Mut} - \Delta G_{WT}$. The protocol reports the total composite ΔΔG (Table S1A), as well as the relative contributions of each energetic component (see Table S1B).

Preparation of Recombinant Plasmids.

A pcDNA5 FRT expression vector bearing a human rhodopsin cDNA insert with an N-terminal influenza hemagglutinin (HA) epitope upstream of the internal ribosome entry site (IRES) and Dasher GFP was used to drive transient rhodopsin expression in conjunction

with bicistronic GFP expression. Mutations were introduced into this construct using site-directed mutagenesis. TEV-cleavable rhodopsin fusion proteins were produced in a version of this construct lacking the IRES-Dasher GFP cassette by introducing a consensus TEV proteolysis site followed by a P-reporter domain (142 residue C-terminal fragment of bovine prolactin) at the 3′ of the rhodopsin gene using Gibson assembly. Plasmids used for transient expression in mammalian cells or for in vitro translation were produced using the Zymopure Midiprep Kit (Zymo Research, Irvine, CA).

In Vitro Translation and Topological Mapping of Rhodop-sin Variants.

A cleavable rhodopsin fusion protein bearing a C- terminal TEV proteolysis site followed by a P-reporter domain was used in conjunction with a proteolytic susceptibility assay[31] in order to characterize the topological orientation of TM7 of nascent rhodopsin variants expressed in canine rough microsomes (tRNA probes, College Station, TX). mRNA for each cleavable rhodopsin variant was produced using the RiboMAX RNA production system (Promega, Madison, WI). Rhodopsin constructs were then expressed from the mRNA using rabbit reticulocyte lysate (Promega, Madison, WI) and canine rough microsomes in accordance with the manufacturer's instructions. Nascent proteins were labeled using EasyTag ^{35}S-labeled methionine (PerkinElmer, Waltham, MA). Following translation, nascent proteins were digested with 20 units of TEV protease (Sigma-Aldrich, St. Louis, MO) per 30 μL lysate for 2 h at 25 °C in the presence and absence of 1% triton X-100 detergent. Samples were then diluted 1:4 into 1X SDS-PAGE sample buffer, then separated on a 12% SDS PAGE gel. Gels were then dried, exposed on a phosphorimaging plate overnight (GE Healthcare, New York, NY), and imaged using a Typhoon Imager (GE Healthcare, New York, NY). Densitometry was used to determine the fraction of protein with native topology by comparison of the intensity of the intact rhodopsin band following digest in the presence and absence of Triton X-100.

Cellular Trafficking of Rhodopsin Variants.

Differential immunostaining of plasma membrane and intracellular rhodopsin was used in conjunction with flow cytometry to characterize the cellular trafficking of rhodopsin variants in a manner described previously.[6] Briefly, rhodopsin variants were transiently expressed in HEK293 cells using Lipofectamine 3000 (Invitrogen, Carlsbad, CA), then harvested 2 days post transfection using Trypsin (Gibco, Grand Island, NY). Rhodopsin proteins at the plasma membrane were then immunostained using a Dylight550-conjugated anti-HA antibody (Invitrogen, Carlsbad, CA) for 30 min in the dark. Cells were then fixed using the Fix and Perm kit (Invitrogen, Carlsbad, CA) in accordance with the manufacturer's instructions. Following fixation, the cells were washed twice with phosphate buffered saline (PBS) containing 5% FBS and 0.1% sodium azide (wash buffer), then permeabilized using the Fix and Perm kit in accordance with the manufacturer's instructions. The remaining intracellular rhodopsin was then immunostained with an Alexa Fluor 647-conjugated anti-HA antibody (Invitrogen, Carlsbad, CA) for 30 min in the dark at room temperature. Cells were then washed twice using wash buffer, then resuspended in wash buffer and filtered prior to analysis. Cellular fluorescence profiles were analyzed using a BD LSRII flow cytometer (BD Biosciences, Franklin Lakes, NJ), and analysis of cellular fluorescence profiles was carried out using FlowJo (Treestar, Ashland, OR). Positively transfected cells

expressing the rhodopsin variants of interest were identified based on the bicistronic expression of Dasher GFP. Single color controls revealed no appreciable spill over between the immunofluorescence signals and/or the bicistronic Dasher GFP. Export efficiency measurements were derived from independent triplicate measurements that were carried out on cells that were at a uniform passage number (p2).

Purification, Regeneration, and Spectral Characterization of Rhodopsin Variants.

Human WT, S297L, S297A, and S297W rhodopsins were transiently expressed in HEK293 cells by polyethylenimine transfection. Cells from 15 10 cm plates were harvested 48 h post transfection and centrifuged at 800g. The cell pellets were then resuspended in 20 mM Bis-tris propane (BTP, pH 7.5) containing 120 mM NaCl and a protease inhibitor cocktail. 11-cis-Retinal was then added to the cell suspension at a final concentration of 10 μM prior to incubation on a rotating platform in the dark for 2 h at 4 °C. Cellular membranes were then solubilized by adding 20 mM *n*-dodecyl-β-D-maltopyranoside (DDM) to the cell suspension and rotating the suspension for an additional hour at 4 °C. The lysate then was centrifuged at 100 000g for 1 h at 4 °C to remove insoluble debris. Rhodopsins were then purified from the supernatant by immunoaffinity chromatography using a monoclonal antibody directed against the C-terminus of rhodopsin (1D4) that was immobilized on cyanogen bromide-activated agarose. 200 μL of 6 mg 1D4/mL agarose beads were added to the supernatant and rotated for 1 h at 4 °C. The resin was then transferred to a column and washed with 10 mL of 20 mM BTP (pH 7.5) containing 120 mM NaCl and 2 mM DDM. Regenerated rhodopsins were then eluted with 20 mM BTP (pH 7.5) containing 120 mM NaCl, 2 mM DDM, and 0.6 mg/mL of an elution peptide (TETSQVAPA).[64] The concentrations of purified rhodopsins were determined assuming a molar extinction coefficient of 40 600 M^{-1} cm^{-1} at 498 nm. UV− visible spectra of rhodopsin variants were recorded in the dark using a Cary 50 UV−visible spectrophotometer (Varian, Palo Alto, CA). The sensitivity of each rhodopsin variant to light was assessed by illumination using a Fiber-Light illuminator (150 W lamp) (Dolan-Jenner, Boxborough, MA) coupled with a band-pass wavelength filter (480−520 nm) at a distance of 15 cm for 5 min. UV−visible spectra were recorded at room temperature immediately after the bleaching procedure.

Chromophore Release.

The release of 11-*cis*-retinal chromo-phore from rhodopsin variants following illumination was measured with a PerkinElmer L55 Fluorescence Spectrometer at 20 °C. All measurements were performed on a 25 nM purified rhodopsin solution containing 20 mM BTP (pH 6.0), 100 mM NaCl, and 1 mM DDM. Samples were illuminated with a Fiber-Light illuminator through a 420−520 nm band-pass filter for 15 s at a distance of 15 cm immediately prior to fluorescence measurements. Spectrofluorometer slit settings were 8 at 295 nm for excitation, and 10 at 330 nm for emission collection. Changes in the intrinsic Trp fluorescence were recorded for 30 min. An increase of the intrinsic Trp fluorescence correlates with the decrease in the protonated Schiff base concentration.[41] All measurements were performed in triplicate.

Activation of G_t by Rhodopsin Variants.

G_t was extracted and purified from rod outer segment (ROS) membranes isolated from 100 dark-adapted bovine retinas[65] as described previously.[66] Purified G_t was then mixed with purified human rhodopsins at a 10:1 ratio (v/v) to final concentrations 250 nM for G_t and 25 nM rhodopsin prior to bleaching of the samples for 30 s using a Fiber-Light illuminator coupled with a band-pass wavelength filter (480−520 nm). After bleaching, the samples were allowed to equilibrate for 200 s with continuous low-speed stirring. The activation kinetics of purified human rhodopsin variants were then monitored using a tryptophan fluorescence-based G_t activation assay. Briefly, a PerkinElmer LS 55 Luminescence Spectrophotometer was used to monitor changes in intrinsic tryptophan fluorescence (300 nm excitation, 345 nm emission) associated with the exchange of guanylyl nucleotide upon addition of 5 μM GTPγS.[67] No change in fluorescence was observed in samples containing rhodopsin in the absence of G_t. All samples were measured in triplicate.

Supplementary Material

Refer to Web version on PubMed Central for supplementary material.

ACKNOWLEDGMENTS

We would like to thank Stephen White, Charles Sanders, Megan Thielges, and David Clemmer for critical reading of the manuscript. This research was supported in part by grants from the National Institutes of Health (NIH) R01 GM129261 to J.P.S. and EY025214 to B.J. Francis J. Roushar gratefully acknowledges receipt of a predoctoral fellowship from the Graduate Training Program in Quantitative and Chemical Biology at Indiana University (T32 GM109825). We thank Christiane Hassel and the Indiana University Bloomington Flow Cytometry Core Facility for their experimental support.

REFERENCES

(1). Wiseman RL; Koulov A; Powers E; Kelly JW; Balch WE Protein energetics in maturation of the early secretory pathway. Curr. Opin. Cell Biol 2007, 19, 359–367. [PubMed: 17686625]

(2). Coppinger JA; Hutt DM; Razvi A; Koulov AV; Pankow S; Yates JR III; Balch WE A chaperone trap contributes to the onset of cystic fibrosis. PLoS One 2012, 7, No. e37682. [PubMed: 22701530]

(3). Pankow S; Bamberger C; Calzolari D; Martínez-Bartolome S; Lavalleé-Adam M; Balch WE; Yates JR F508 CFTR interactome remodelling promotes rescue of cystic fibrosis. Nature 2015, 528, 510–516. [PubMed: 26618866]

(4). El-Kasaby A; Koban F; Sitte HH; Freissmuth M; Sucic S A cytosolic relay of heat shock proteins HSP70−1A and HSP90beta monitors the folding trajectory of the serotonin transporter. J. Biol. Chem 2014, 289, 28987–29000. [PubMed: 25202009]

(5). Schlebach JP; Sanders CR The safety dance: biophysics of membrane protein folding and misfolding in a cellular context. Q. Rev. Biophys 2015, 48, 1–34. [PubMed: 25420508]

(6). Schlebach JP; Narayan M; Alford C; Mittendorf KF; Carter BD; Li J; Sanders CR Conformational Stability and Pathogenic Misfolding of the Integral Membrane Protein PMP22. J. Am. Chem. Soc 2015, 137, 8758–8768. [PubMed: 26102530]

(7). Sanders C; Myers J Disease-related misassembly of membrane proteins. Annu. Rev. Biophys. Biomol. Struct 2004, 33, 25–51. [PubMed: 15139803]

(8). Sakakura M; Hadziselimovic A; Wang Z; Schey KL; Sanders CR Structural basis for the Trembler-J phenotype of Charcot-Marie-Tooth disease. Structure 2011, 19, 1160–1169. [PubMed: 21827951]

(9). Huang H; Kuenze G; Smith JA; Taylor KC; Duran AM; Hadziselimovic A; Meiler J; Vanoye CG; George AL Jr.; Sanders CR Mechanisms of KCNQ1 channel dysfunction in long QT syndrome involving voltage sensor domain mutations. Sci. Adv 2018, 4, No. eaar2631. [PubMed: 29532034]

(10). Placone J; Hristova K Direct assessment of the effect of the Gly380Arg achondroplasia mutation on FGFR3 dimerization using quantitative imaging FRET. PLoS One 2012, 7, No. e46678. [PubMed: 23056398]

(11). Schlebach JP; Sanders CR Influence of Pathogenic Mutations on the Energetics of Translocon-Mediated Bilayer Integration of Transmembrane Helices. J. Membr. Biol 2015, 248, 371–381. [PubMed: 25192979]

(12). Kim SJ; Skach WR Mechanisms of CFTR Folding at the Endoplasmic Reticulum. Front. Pharmacol 2012, 3, 201. [PubMed: 23248597]

(13). Buck TM; Skach WR Differential stability of biogenesis intermediates reveals a common pathway for aquaporin-1 topological maturation. J. Biol. Chem 2005, 280, 261–269. [PubMed: 15516332]

(14). Feige MJ; Hendershot LM Quality control of integral membrane proteins by assembly-dependent membrane integration. Mol. Cell 2013, 51, 297–309. [PubMed: 23932713]

(15). Kelly JW; Balch WE The integration of cell and chemical biology in protein folding. Nat. Chem. Biol 2006, 2, 224–227. [PubMed: 16619016]

(16). Hessa T; Meindl-Beinker NM; Bernsel A; Kim H; Sato Y; Lerch-Bader M; Nilsson I; White SH; von Heijne G Molecular code for transmembrane-helix recognition by the Sec61 translocon. Nature 2007, 450, 1026–1030. [PubMed: 18075582]

(17). Öjemalm K; Higuchi T; Jiang Y; Langel Ü; Nilsson I; White SH; Suga H; von Heijne G Apolar surface area determines the efficiency of translocon-mediated membrane-protein integration into the endoplasmic reticulum. Proc. Natl. Acad. Sci. U. S. A 2011, 108, E359–364. [PubMed: 21606334]

(18). Öjemalm K; Higuchi T; Lara P; Lindahl E; Suga H; von Heijne G Energetics of side-chain snorkeling in transmembrane helices probed by nonproteinogenic amino acids. Proc. Natl. Acad. Sci. U. S. A 2016, 113, 10559–10564. [PubMed: 27601675]

(19). Heinrich SU; Mothes W; Brunner J; Rapoport TA The Sec61p complex mediates the integration of a membrane protein by allowing lipid partitioning of the transmembrane domain. Cell 2000, 102, 233–244. [PubMed: 10943843]

(20). Gafvelin G; von Heijne G Topological ″frustration″ in multispanning E. coli inner membrane proteins. Cell 1994, 77, 401–412. [PubMed: 8181060]

(21). Kauko A; Hedin LE; Thebaud E; Cristobal S; Elofsson A; von Heijne G Repositioning of transmembrane alpha-helices during membrane protein folding. J. Mol. Biol 2010, 397, 190–201. [PubMed: 20109468]

(22). Lu Y; Turnbull IR; Bragin A; Carveth K; Verkman AS; Skach WR Reorientation of aquaporin-1 topology during maturation in the endoplasmic reticulum. Mol. Biol. Cell 2000, 11, 2973–2985. [PubMed: 10982394]

(23). Virkki MT; Agrawal N; Edsbacker E; Cristobal S; Elofsson A; Kauko A Folding of Aquaporin 1: Multiple evidence that helix 3 can shift out of the membrane core. Protein Sci 2014, 23, 981–992. [PubMed: 24777974]

(24). Öjemalm K; Halling KK; Nilsson I; von Heijne G Orientational preferences of neighboring helices can drive ER insertion of a marginally hydrophobic transmembrane helix. Mol. Cell 2012, 45, 529–540. [PubMed: 22281052]

(25). Moss K; Helm A; Lu Y; Bragin A; Skach WR Coupled translocation events generate topological heterogeneity at the endoplasmic reticulum membrane. Mol. Biol. Cell 1998, 9, 2681–2697. [PubMed: 9725920]

(26). Van Lehn RC; Zhang B; Miller TF III Regulation of multispanning membrane protein topology via post-translational annealing. eLife 2015, 4, No. e08697. [PubMed: 26408961]

(27). Tzekov R; Stein L; Kaushal S Protein misfolding and retinal degeneration. Cold Spring Harbor Perspect. Biol 2011, 3, a007492.

(28). Wimley WC; Creamer TP; White SH Solvation energies of amino acid side chains and backbone in a family of host-guest pentapeptides. Biochemistry 1996, 35, 5109–5124. [PubMed: 8611495]

(29). Hessa T; Kim H; Bihlmaier K; Lundin C; Boekel J; Andersson H; Nilsson I; White SH; von Heijne G Recognition of transmembrane helices by the endoplasmic reticulum translocon. Nature 2005, 433, 377–381. [PubMed: 15674282]

(30). Elazar A; Weinstein JJ; Prilusky J; Fleishman SJ Interplay between hydrophobicity and the positive-inside rule in determining membrane-protein topology. Proc. Natl. Acad. Sci. U. S. A 2016, 113, 10340–10345. [PubMed: 27562165]

(31). Skach WR Topology of P-glycoproteins. Methods Enzymol 1998, 292, 265–278. [PubMed: 9711560]

(32). Hermansson M; von Heijne G Inter-helical hydrogen bond formation during membrane protein integration into the ER membrane. J. Mol. Biol 2003, 334, 803–809. [PubMed: 14636604]

(33). Meindl-Beinker NM; Lundin C; Nilsson I; White SH; von Heijne G Asn- and Asp-mediated interactions between transmembrane helices during translocon-mediated membrane protein assembly. EMBO Rep 2006, 7, 1111–1116. [PubMed: 17008929]

(34). Moon CP; Fleming KG Side-chain hydrophobicity scale derived from transmembrane protein folding into lipid bilayers. Proc. Natl. Acad. Sci. U. S. A 2011, 108, 10174–10177. [PubMed: 21606332]

(35). McDonald SK; Fleming KG Aromatic Side Chain Water-to-Lipid Transfer Free Energies Show a Depth Dependence across the Membrane Normal. J. Am. Chem. Soc 2016, 138, 7946–7950. [PubMed: 27254476]

(36). Elazar A; Weinstein J; Biran I; Fridman Y; Bibi E; Fleishman SJ Mutational scanning reveals the determinants of protein insertion and association energetics in the plasma membrane. eLife 2016, 5, No. e12125.

(37). Noorwez SM; Malhotra R; McDowell JH; Smith KA; Krebs MP; Kaushal S Retinoids assist the cellular folding of the autosomal dominant retinitis pigmentosa opsin mutant P23H. J. Biol. Chem 2004, 279, 16278–16284. [PubMed: 14769795]

(38). Tian H; Sakmar TP; Huber T The Energetics of Chromophore Binding in the Visual Photoreceptor Rhodopsin. Biophys. J 2017, 113, 60–72. [PubMed: 28700926]

(39). Fluman N; Tobiasson V; von Heijne G Stable membrane orientations of small dual-topology membrane proteins. Proc. Natl. Acad. Sci. U. S. A 2017, 114, 7987–7992. [PubMed: 28698365]

(40). Kaushal S; Khorana HG Structure and function in rhodopsin. 7. Point mutations associated with autosomal dominant retinitis pigmentosa. Biochemistry 1994, 33, 6121–6128. [PubMed: 8193125]

(41). Farrens DL; Khorana HG Structure and function in rhodopsin. Measurement of the rate of metarhodopsin II decay by fluorescence spectroscopy. J. Biol. Chem 1995, 270, 5073–5076. [PubMed: 7890614]

(42). Heck M; Hofmann KP Maximal rate and nucleotide dependence of rhodopsin-catalyzed transducin activation: initial rate analysis based on a double displacement mechanism. J. Biol. Chem 2001, 276, 10000–10009. [PubMed: 11116153]

(43). Marshall SS; Niesen MJM; Müller A; Tiemann K; Saladi SM; Galimidi RP; Zhang B; Clemons WM Jr.; Miller TF III A link between integral membrane protein expression and simulated integration efficiency. Cell Rep 2016, 16, 2169–2177. [PubMed: 27524616]

(44). Niesen MJM; Marshall SS; Miller TF III; Clemons WM Jr. Improving membrane protein expression by optimizing integration efficiency. J. Biol. Chem 2017, 292, 19537–19545. [PubMed: 28918393]

(45). Popot JL; Engelman DM Helical membrane protein folding, stability, and evolution. Annu. Rev. Biochem 2000, 69, 881–922. [PubMed: 10966478]

(46). von Heijne G Membrane protein structure prediction. Hydrophobicity analysis and the positive-inside rule. J. Mol. Biol 1992, 225, 487–494. [PubMed: 1593632]

(47). Chen Y; Chen Y; Jastrzebska B; Golczak M; Gulati S; Tang H; Seibel W; Li X; Jin H; Han Y; Gao S; Zhang J; Liu X; Heidari-Torkabadi H; Stewart PL; Harte WE; Tochtrop GP; Palczewski K A novel small molecule chaperone of rod opsin and its potential therapy for retinal degeneration. Nat. Commun 2018, 9, 1976. [PubMed: 29773803]

(48). Chen Y; Jastrzebska B; Cao P; Zhang J; Wang B; Sun W; Yuan Y; Feng Z; Palczewski K Inherent Instability of the Retinitis Pigmentosa P23H Mutant Opsin. J. Biol. Chem 2014, 289, 9288–9303. [PubMed: 24515108]

(49). Bernier V; Lagace M; Bichet DG; Bouvier M Pharmacological chaperones: potential treatment for conformational diseases. Trends Endocrinol. Metab 2004, 15, 222–228. [PubMed: 15223052]

(50). Powers ET; Morimoto RI; Dillin A; Kelly JW; Balch WE Biological and chemical approaches to diseases of proteostasis deficiency. Annu. Rev. Biochem 2009, 78, 959–991. [PubMed: 19298183]

(51). Ren HY; Grove DE; De La Rosa O; Houck SA; Sopha P; Van Goor F; Hoffman BJ; Cyr DM VX-809 corrects folding defects in cystic fibrosis transmembrane conductance regulator protein through action on membrane-spanning domain 1. Mol. Biol. Cell 2013, 24, 3016–3024. [PubMed: 23924900]

(52). Veit G; Avramescu RG; Chiang AN; Houck SA; Cai Z; Peters KW; Hong JS; Pollard HB; Guggino WB; Balch WE; Skach WR; Cutting GR; Frizzell RA; Sheppard DN; Cyr DM; Sorscher EJ; Brodsky JL; Lukacs GL From CFTR biology toward combinatorial pharmacotherapy: expanded classification of cystic fibrosis mutations. Mol. Biol. Cell 2016, 27, 424–433. [PubMed: 26823392]

(53). Wainwright CE; Elborn JS; Ramsey BW Lumacaftor-Ivacaftor in Patients with Cystic Fibrosis Homozygous for Phe508del CFTR. N. Engl. J. Med 2015, 373, 1783–1784.

(54). Rowe SM; Daines C; Ringshausen FC; Kerem E; Wilson J; Tullis E; Nair N; Simard C; Han L; Ingenito EP; McKee C; Lekstrom-Himes J; Davies JC Tezacaftor-Ivacaftor in Residual-Function Heterozygotes with Cystic Fibrosis. N. Engl. J. Med 2017, 377, 2024–2035. [PubMed: 29099333]

(55). Taylor-Cousar JL; Munck A; McKone EF; van der Ent CK; Moeller A; Simard C; Wang LT; Ingenito EP; McKee C; Lu Y; Lekstrom-Himes J; Elborn JS Tezacaftor-Ivacaftor in Patients with Cystic Fibrosis Homozygous for Phe508del. N. Engl. J. Med 2017, 377, 2013–2023. [PubMed: 29099344]

(56). Taverna DM; Goldstein RA Why are proteins marginally stable? Proteins: Struct., Funct., Genet 2002, 46, 105–109. [PubMed: 11746707]

(57). Janovick JA; Knollman PE; Brothers SP; Ayala-Yañez R; Aziz AS; Conn PM Regulation of G protein-coupled receptor trafficking by inefficient plasma membrane expression: molecular basis of an evolved strategy. J. Biol. Chem 2006, 281, 8417–8425. [PubMed: 16446355]

(58). Conn PM; Janovick JA; Brothers SP; Knollman PE 'Effective inefficiency': cellular control of protein trafficking as a mechanism of post-translational regulation. J. Endocrinol 2006, 190, 13–16. [PubMed: 16837606]

(59). Wiseman RL; Powers ET; Buxbaum JN; Kelly JW; Balch WE An adaptable standard for protein export from the endoplasmic reticulum. Cell 2007, 131, 809–821. [PubMed: 18022373]

(60). Song Y; DiMaio F; Wang RY; Kim D; Miles C; Brunette T; Thompson J; Baker D High-resolution comparative modeling with RosettaCM. Structure 2013, 21, 1735–1742. [PubMed: 24035711]

(61). Simons KT; Kooperberg C; Huang E; Baker D Assembly of protein tertiary structures from fragments with similar local sequences using simulated annealing and Bayesian scoring functions. J. Mol. Biol 1997, 268, 209–225. [PubMed: 9149153]

(62). Lomize MA; Lomize AL; Pogozheva ID; Mosberg HI OPM: orientations of proteins in membranes database. Bioinformatics 2006, 22, 623–625. [PubMed: 16397007]

(63). Kellog EH; Leaver-Fay A; Baker D Role of conformational sampling in computing mutation-induced changes in protein structure and stability. Proteins: Struct., Funct., Genet 2011, 79, 830–838. [PubMed: 21287615]

(64). Salom D; Le Trong I; Pohl E; Ballesteros JA; Stenkamp RE; Palczewski K Improvements in G protein-coupled receptor purification yield light stable rhodopsin crystals. J. Struct. Biol 2006, 156, 497–504. [PubMed: 16837211]

(65). Papermaster DS Preparation of retinal rod outer segments. Methods Enzymol 1982, 81, 48–52. [PubMed: 6212746]

(66). Jastrzebska B Oligomeric state of rhodopsin within rhodopsin-transducin complex probed with succinylated concanavalin A. Methods Mol. Biol 2015, 1271, 221–233. [PubMed: 25697527]

(67). Fahmy K; Sakmar TP Regulation of the rhodopsin-transducin interaction by a highly conserved carboxylic acid group. Biochemistry 1993, 32, 7229–7236. [PubMed: 8343512]

(68). Jastrzebska B; Maeda T; Zhu L; Fotiadis D; Filipek S; Engel A; Stenkamp RE; Palczewski K Functional characterization of rhodopsin monomers and dimers in detergents. J. Biol. Chem 2004, 279, 54663–54675. [PubMed: 15489507]

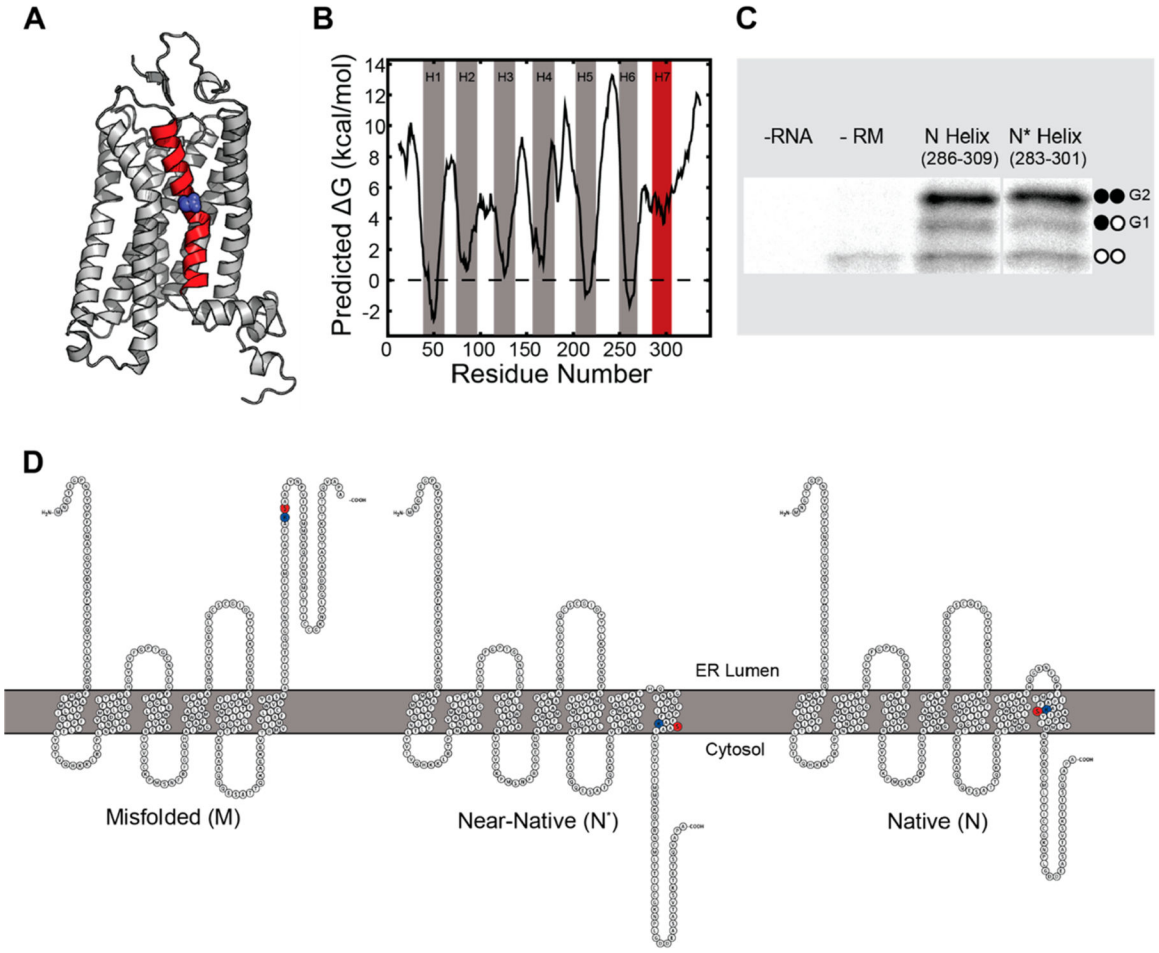

Figure 1.

Topological energetics of rhodopsin. Sequence-based predictions of the topological energetics of human rhodopsin are analyzed in relation to its native structure. (A) A structural model of human rhodopsin is shown from the plane of the membrane. The seventh transmembrane domain is shown in red for reference. The side chain of residue 297 is depicted with blue spheres. (B) The predicted transfer free energy for each 23-amino acid segment of rhodopsin, which was calculated using the ΔG predictor algorithm,[16] is plotted against the central position of each corresponding segment. The positions of the energetic minima corresponding to the first six predicted transmembrane domains called by the algorithm are indicated in gray. The approximate position of the seventh transmembrane domain is marked in red. (C) Chimeric Lep proteins containing the native (residues 286−309) and near-native (residues 283−301) segments of TM7 were produced by in vitro translation in the presence of canine rough microsomes and separated by SDS-PAGE. Lanes from left to right depict the following reactions: (1) negative control containing no RNA, (2) negative control containing RNA but no rough microsomes, (3) reaction containing RNA for the Lep construct containing the native helix and rough microsomes, and (4) reaction containing RNA for the Lep construct containing the near-native helix and rough microsomes. The positions of the untargeted and the singly (G1, membrane integrated TM7) and doubly (G2, aqueous TM7) glycosylated bands are indicated for reference. (D) A

cartoon depicts the orientation of the rhodopsin sequence with respect to the membrane for the two most probable predicted topologies according to TopGraph,[30] which we have termed the misfolded (M, left) and near-native (N*, center) states. A third state in which the seventh transmembrane domain has shifted to its native topology, which we have termed the native state (N, right), is also shown for reference. K296, which forms a Schiff base with retinal, is shown in blue. S297 is shown in red.

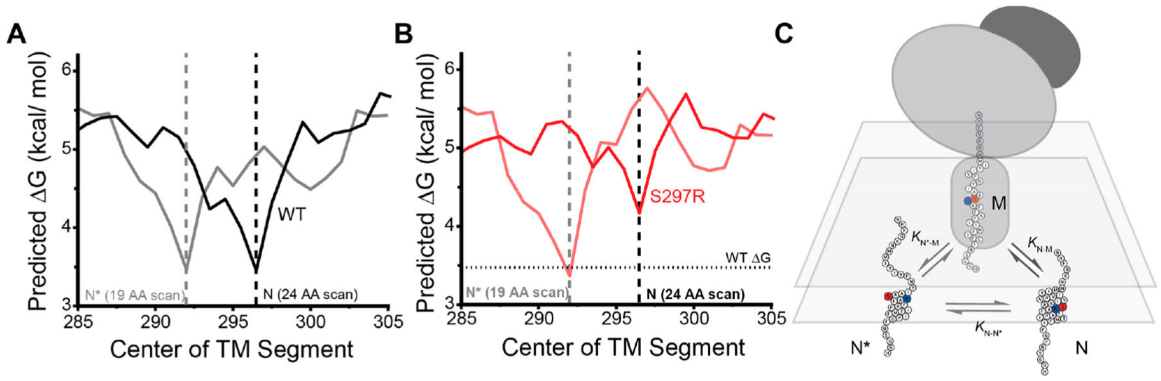

Figure 2.

Modeling the effects of mutations on the topological energetics of rhodopsin. Sequence scans provide computation estimates for the effects of mutations on the nascent topological ensemble of transmembrane domain 7 (TM7). (A) The TM7 region of WT rhodopsin was scanned with 24-residue (black) and 19-residue (gray) windows using the ΔG predictor,[16] and the predicted free energy difference associated with the translocon-mediated membrane integration of the nascent chain is plotted as a function of the central position of the TM segment. (B) The TM7 region of S297R rhodopsin was scanned with 24-residue (red) and 19-residue (pink) windows using the ΔG predictor,[16] and the predicted free energy difference associated with the translocon-mediated membrane integration of the nascent chain is plotted as a function of the central position of the TM segment. (C) A cartoon depicts the manner in which a three state equilibrium model can be applied to rationalize the nascent topological ensemble of TM7.

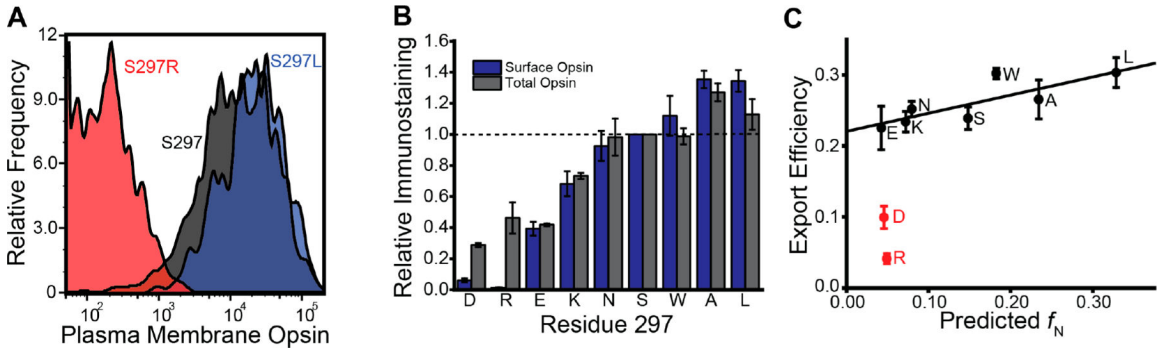

Figure 3.

Cellular expression and trafficking of engineered rhodopsin variants. Selective immunostaining of surface and intracellular opsin was employed in conjunction with flow cytometry to measure the proteostatic effects of mutations. (A) A histogram depicts the distribution of cellular fluorescence intensities associated with the immunostaining of opsin at the plasma membrane of HEK293 cells transiently expressing WT (black), S297L (blue), and S297R (red) opsin as determined by flow cytometry. (B) The average fluorescence intensities associated with the immunostaining of plasma membrane opsin (blue) and total cellular opsin (gray) for HEK293 cells expressing rhodopsin variants was normalized relative to that of WT. The average value from three biological replicates is shown. Error bars reflect standard deviations. (C) The average fraction of cellular opsin at the plasma membrane (export efficiency) calculated from three biological replicates for each variant is plotted against the predicted fraction of native topomer (see Supplemental Theory). A linear fit of all variants except for S297D and S297R is shown for reference.

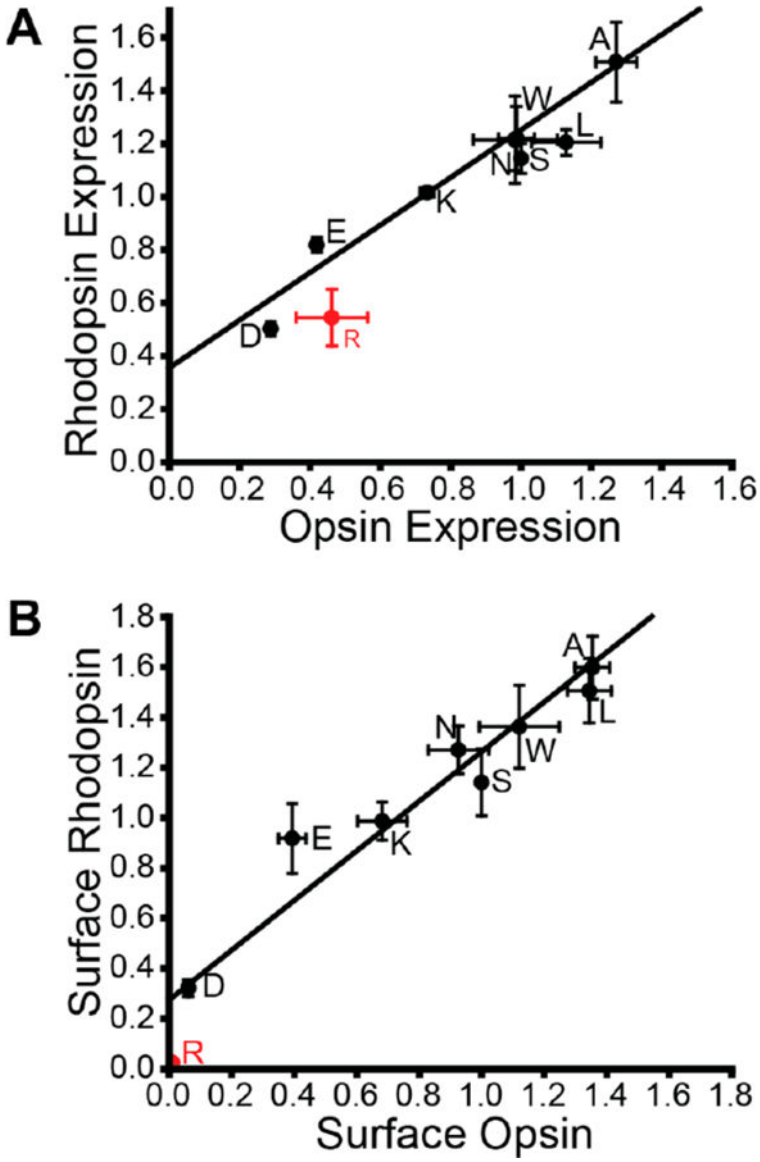

Figure 4.

Influence of retinal on the cellular expression and trafficking of engineered rhodopsin variants. (A) The effects of mutations at residue 297 on the expression level was compared in the presence (rhodopsin, Y-axis) and absence (opsin, X-axis) of 5 μM 9-*cis*-retinal. Total protein immunostaining levels are normalized relative to that of WT in the absence of retinal. A linear fit for all of the variants except S297R is shown for reference (Pearson's R = 0.95). The slope of the line of best fit was 0.9 ± 0.1. (B) The effects of mutations at residue 297 on the surface immunostaining was compared in the presence (rhodopsin, Y-axis) and absence (opsin, X-axis) of 5 μM 9-*cis*-retinal. Surface immunostaining levels are normalized relative to that of WT in the absence of retinal. A linear fit for all of the variants except S297R is shown for reference (Pearson's R = 0.99). The slope of the line of best fit was 0.99 ± 0.06.

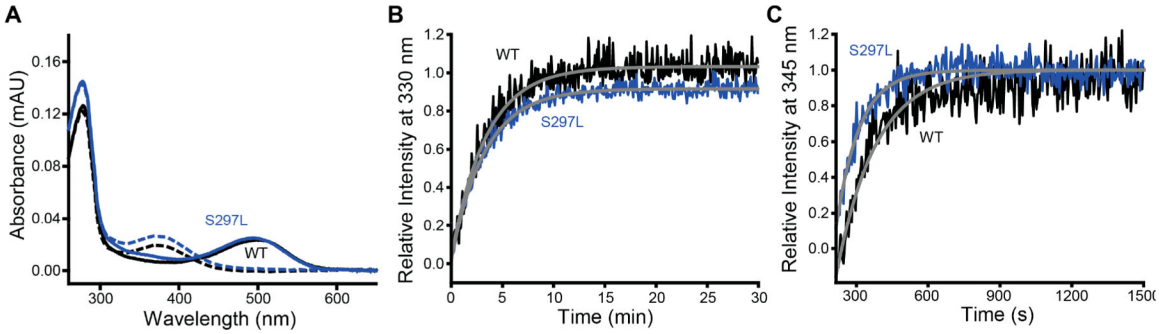

Figure 5.

Functional properties of S297L rhodopsin. The absorbance spectra, chromophore release kinetics, and G_t activation kinetics of purified WT and S297L rhodopsin were characterized in vitro. (A) The UV−visible absorbance spectra of WT (black) and S297L (blue) rhodopsin are shown before (solid) and after (dashes) exposure to light. (B) The kinetics of retinal release following photoactivation of rhodopsin were monitored using the change in fluorescence intensity at 330 nm.[41,68] The normalized fluorescence intensity associated with the release of retinal by WT (black) and S297L (blue) rhodopsin is plotted against time. (C) Purified G_t protein was mixed with rhodopsins, and the kinetics of G_t activation were monitored by the change in fluorescence over time associated with nucleotide exchange.[67] The normalized fluorescence intensity associated with the activation of G_t by WT (black) and S297L (blue) rhodopsin is plotted against time. Each measurement was carried out in triplicate.

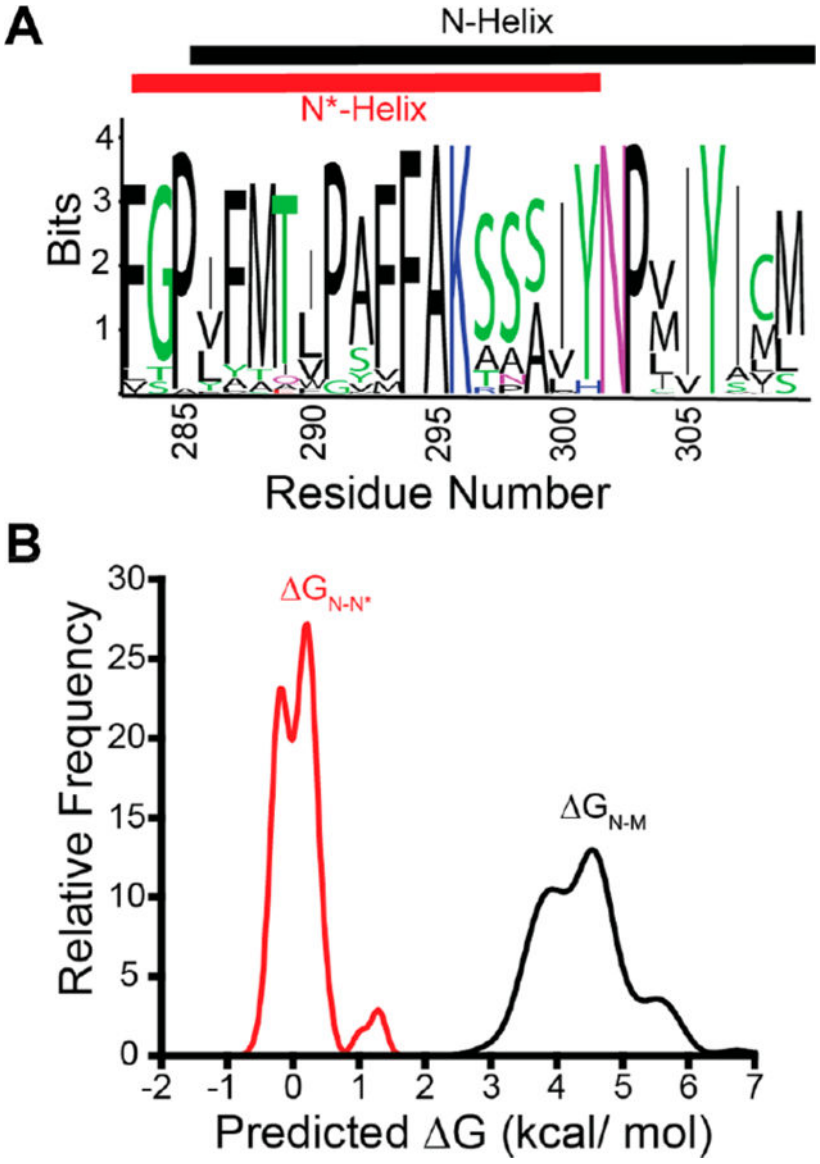

Figure 6.

Evolutionary constraints on the topological energetics of transmembrane domain 7. The sequences of the seventh trans-membrane domain (TM7) from 104 related rhodopsin proteins are compared with respect to their predicted topological energetics. (A) A sequence logo plot depicts the relative frequencies of amino acids at each residue in TM7 among related rhodopsin proteins. The relative sizes of the letters indicate their frequency among the sequences. Bars indicate the position of TM7 in the N state (black) and in the N* state (red). (B) A histogram depicts the distribution of predicted free energy differences between the misfolded (M) and native (N) topological states (black) as well as the predicted free energy differences between the near-native (N*) and native (N) topological states as determined using the ΔG predictor algorithm.[16]

Table 1.

Cellular Trafficking of Rhodopsin Variants

	energetic predictions			cellular immunostaining	
variant	**predicted $\Delta\Delta G_{N-M}$ (kcal/mol)[a]**	**predicted $\Delta\Delta G_{N^*-M}$ (kcal/mol)[b]**	**predicted fraction of native topomer[c]**	**relative surface immunostaining**	**relative total immunostaining**
S297L	−0.84	−0.75	0.32	1.34 ± 0.07	1.1 ± 0.1
S297A	−0.43	−0.39	0.23	1.35 ± 0.06	1.27 ± 0.06
S297W	−0.33	−0.65	0.18	1.1 ± 0.1	0.99 ± 0.05
WT	–	–	0.14	–	–
S297N	0.47	0.37	0.08	0.9 ± 0.1	1.0 ± 0.1
S297K	0.87	0.38	0.04	0.68 ± 0.08	0.73 ± 0.02
S297E	0.54	0.46	0.07	0.39 ± 0.04	0.42 ± 0.01
S297D	0.83	0.44	0.04	0.06 ± 0.01	0.29 ± 0.01
S297R	0.71	−0.09	0.05	0.01 ± 0.001	0.5 ± 0.1

[a] Predicted $\Delta\Delta G_{N-M}$ values were determined by subtracting the minimum predicted ΔG for membrane integration for WT from that of each mutant based on a 24-residue window scan using the ΔG predictor.

[b] Predicted $\Delta\Delta G_{N^*-M}$ values were determined by subtracting the minimum predicted ΔG for membrane integration for WT from that of each variant based on a 19-residue window scan using the ΔG predictor.

[c] See Supplemental Theory for derivation of these values.

Table 2.

Functional Properties of Rhodopsin Variants

variant	chromophore regeneration efficiency (A_{280}/A_{496})[a]	apparent *k* ($\times 10^{-3}$ s^{-1}) meta II decay[b]	apparent k ($\times 10^{-3}$ s^{-1}) G_t activation[b]
WT	3.9	4.4 ± 0.7	7.4 ± 0.2
S297L	3.8	4.6 ± 0.6	6.5 ± 0.5
S297A	5.4	2.6 ± 0.5	5.3 ± 0.6
S297W	7.1	1.4 ± 0.2	N/A[c]

[a] Higher values indicate a lower yield of regenerated chromophore.

[b] Values represent the average of three experimental replicates, and the error reflects the standard deviation.

[c] Little change in the signal was observed over time.